Interpenetrated Luminescent Metal-Organic Frameworks based on 1H-Indazole-5-carboxylic Acid

Antonio A. García-Valdivia,[a] Manuel Pérez-Mendoza,[a] Javier Cepeda,[b,] Belén Fernández,[c] Manuel Souto,[d,e] Marcos González,[a] José A. García,[f] Guillermo Mínguez Espallargas,[d,*] and Antonio Rodríguez-Diéguez[a,*]*

[a]Departamento de Química Inorgánica, Universidad de Granada, 18071, Granada, Spain.

[b]Departamento de Química Aplicada, Facultad de Química, Universidad del País Vasco/Euskal Herriko Unibertsitatea, UPV/EHU, 20018, San Sebastián, Spain.

[c]Institute of Parasitology and Biomedicine "Lopéz-Neyra", CSIC, Av. Conocimiento s/n, 18600, Granada, Spain.

[d]Instituto de Ciencia Molecular (ICMol), Universitat de Valencia, c/ Catedrático José Beltrán, 2, 46980, Paterna, Spain.

[e]CICECO -Aveiro Institute of Materials, Department of Chemistry, University of Aveiro, 3810-193 Aveiro, Portugal.

[f]Departamento de Fisica Aplicada II, Facultad de Ciencia y Tecnología, University of Basque Country (UPV/EHU), 48940, Leioa, Spain.

KEYWORDS: 1H-Indazole-5-carboxylic Acid, Metal-Organic Frameworks, MOFs, Luminescence Properties, Phosphorescence.

Abstract

Herein we report the formation and characterization of two novel Zn-based multifunctional metal-organic frameworks (MOFs) based on 1H-indazole-5-carboxylic acid and bipyridine-like linkers, synthesized by soft solvothermal routes. These materials possess isoreticular two-fold interpenetrated 3D-structures which afford a flexible character and allow porosity modulation of the MOFs as confirmed by CO_2 sorption measurements. Apart from this attractive structural feature, the MOFs exhibit fascinating luminescent properties involving both luminescence thermometry and long-lasting phosphorescence.

Introduction

The development of novel functional porous materials is one major point towards the sustainable development of our society and should deal with an optimum performance for the capture, separation and storage of different types of gases at industrial level.[1-3] In this sense, much efforts have been devoted to produce selective adsorbents for purifying and separating CO_2 in the mixture resulting from a gasification process.[4-9] One important research field that has emerged during the last two decades has mainly focused on the design and synthesis of new metal-organic frameworks (MOFs), also called porous coordination polymers (PCPs), which are materials constituted by organic ligands coordinated to metal ions or clusters defining a porous and crystalline network with structural diversities as a consequence of their modular nature and, consequently, functional properties. Therefore, MOFs cover multiple fields of applications in addition to adsorption, such as magnetism, luminescence, electronics, catalysis or medicine.[10,11] An

interesting synthetic strategy to achieve an optimal structure to enhance the gas storage or separation performance is based on the modulation of the size and type of pore in a rational way, by using different ligands that present small structural changes (i.e. the size or shape) to yield topologically similar polymeric materials but with small pore changes. In this sense, the resulting materials may present small modifications that could be, in turn, related to other properties such as luminescence.[12] The enormous family of excellent porous materials synthesized from bipyridine ligands are good examples of such precise pore design and control.[13,14]

Photoluminescence (PL) properties of MOFs have received a lot of interest during the last decade not only because of their large applicability in solid-state lighting materials (light-emitting devices (LEDs), long lasting phosphors (LLPs), and so on)[15-17] but also towards sensing applications due to the celerity of the process. In this last particular case, when luminescent emission is coupled to a physical change such as the temperature, MOFs allow for a rapid detection of that magnitude.[18-20] A main reason for such behaviour is due to the fact that temperature is a key factor in MOFs that governs the non-radiative quenching originated at the molecular vibrations of ligands and, in turn, it brings structural changes of variable magnitude depending on the flexibility of the framework. PL in MOFs takes advantage of their hybrid metal-organic structure since the emissions may involve different components: ligand centred (LC) and metal centred (MC) charge transfers (CT) processes between them, or even be related to the adsorption of guest molecules (which could be exploited for PL detection).[21] However, most of luminescent MOFs used as thermometers are based on lanthanide metals[18-20,(also Cui et al. Chem. Commun. 2015, 51, 7420-7431)] which present some disadvantages such as reduced resources availability and environmental concerns. For this reason, another promising strategy for the

design on luminescent MOFs for thermometry argues for the use of organic ligands with strong absorption (usually molecules with chemical functions containing heteroatoms with lone-pairs) combined with metal ions with closed-shell electronic configuration, which avoid non-radiative quenching.[22,12]

Taking these considerations into account, we selected two different bipyridine ligands and 1H-indazole-5-carboxylic acid (5-incaH) as main ligand, with the aim of obtaining new three-dimensional MOFs. In relation to the latter ligand, there are only few examples of coordination polymers based on copper in which this ligand is acting as a bidentate ligand participating as monoanionic linker (Scheme I, left).[23] Regarding the bipyridine ligands, we have chosen the 4,4-bipyridyl (4,4-bipy) and the 3,6-bis(4-pyridyl)-1,2,4,5-tetrazine (pbptz) as linkers due to the presence of pyridine and tetrazine rings that favor the enhancement of the luminescent properties of the resulting coordination polymers,[24,25] and due to their high potential to build open architectures as a result of the length of the spacer and the disposition of the donor atoms. On the other hand, the linkage of the ligands to metal atoms with a high coordination plasticity, such as zinc (II), opens the way to synthesize materials with not only possible dynamics in the crystal structures but also interesting photoluminescence properties.[12] Moreover, the existence of a second type of ligand that combines benzene with pyrazole rings may modify the initial properties of these systems, generating MOFs with tunable luminescent properties in which the emission of the materials in response to the temperature can be analyzed in order to study their potential use as thermometers, as seen in previous studies conducted on zinc and pyrazole based coordination polymers.[26]

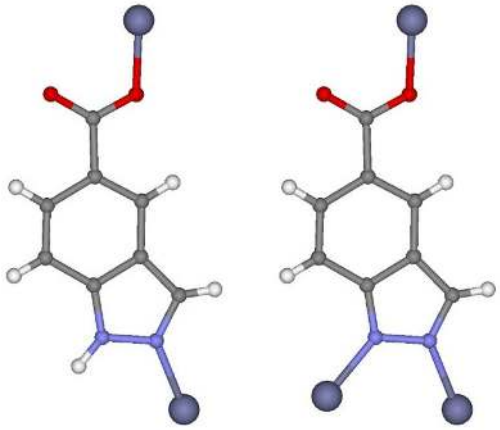

Scheme I. Coordination modes of 5-inca.

Therefore, we report herein the synthesis and characterization of a novel family of Zn^{2+} coordination polymers based on the novel 1H-indazole-5-carboxylic acid, $\{[Zn(5\text{-inca})(pbptz)_{0.5}]\cdot 1.5DMF\}_n$ (**1**) and $\{[Zn(5\text{-inca})(4,4\text{-bipy})_{0.5}]\cdot DMF\}_n$ (**2**). In these compounds, 5-inca ligand shows a new coordination mode (Scheme I, right), by which is coordinated to Zn ions through two nitrogen and one oxygen pertaining to the pyrazole ring and the carboxylate group, respectively. Both materials possess open structures despite the occurrence of interpenetration and are able to adsorb CO_2 with tunable sorption capacities. Photoluminescence measurements together with TD-DFT calculations have been performed in order to verify the origin of the emissions occurring when these ligands are coordinated to d^{10} transition metal ion in the MOFs. Moreover, the emission of the materials in response to the temperature has been analyzed in order to study their potential utility as thermometers due to the presence of pyrazole rings and zinc ions in the frameworks.[26]

Experimental Procedures

Chemicals. All the chemicals were of reagent grade and were used as commercially obtained.

Synthesis {[Zn(5-inca)(pbptz)$_{0.5}$]·1.5 DMF}$_n$ (1). 0.12 mmol (20.00 mg) of 1-H-indazole-5-carboxylate and 0.06 mmol (14.17 mg) of 3,6-di(4-pyridinyl)-1,2,4,5-tetrazine were dissolved in 0.5 mL of DMF and then 0.5 mL of distilled water was added. On the other hand, 0.12 mmol (22.02 mg) of zinc acetate was dissolved in 0.5 mL of distilled water and afterward 0.5 mL of DMF was added. Both solutions were mixed and the resulting solution was placed in a closed glass vessel and heated in an oven at 95 °C for 24 h. Pink single crystals were grown during the heating procedure under autogenous pressure, which were filtered off and collected at open atmosphere and washed with water. Yield: 38% based on zinc. Anal. Calcd. for $C_{18.5}H_{18.5}N_{6.5}O_{3.5}Zn$: C, 49.02; H, 4.11; N, 20.09. Found: C, 48.23; H, 3.31; N, 20.49%.

Synthesis of {[Zn(5-inca)(4,4-bipy)$_{0.5}$]·DMF}$_n$ (2). Well-shaped yellow single crystals of **2** were obtained after carrying out the same general procedure described for **1** but replacing 3,6-di(4-pyridinyl)-1,2,4,5-tetrazine by 4,4´-dipyridil (9.37 mg). Yield: 45% based on zinc. Anal. Calcd. for $C_{16}H_{15}N_4O_3Zn$: C, 51.01; H, 4.01; N, 14.87. Found: C, 50.86; H, 3.98; N, 14.95%.

Physical Measurements. Elemental analyses (C, H, N) were performed on an Euro EA Elemental Analyzer. FTIR spectra (KBr pellets) were recorded on a Nicolet IR 6700 spectrometer in the 4000−400 cm^{-1} spectral region. Thermogravimetric analysis was carried out using a Mettler Toledo TGA/SDTA 851 apparatus in the 25–600 °C temperature range with a 10 °C min^{-1} scan rate and a N_2 flow of 30 mL min^{-1}. High pressure adsorption isotherms have been measured in a non-commercial volumetric adsorption instrument (University of Granada) equipped with two Baratron absolute pressure transducers (MKS type 627B). Their pressure

ranges are from 0 to 133.33 kPa and from 0 to 3333.25 kPa, respectively, and the reading accuracy is 0.05% of the usable measurement range. Prior to measurement, powder samples were heated at 393 K for 12 h and outgassed to 10^{-5} Torr. All gases employed were supplied by Air Liquide with a purity of at least 99.998%. A closed cycle helium cryostat enclosed in an Edinburgh Instruments FLS920spectrometer was employed for steady state photoluminescence (PL) and lifetime measurements at variable temperature. All samples were first placed under high vacuum (of ca. 10^{-9} mbar) to avoid the presence of oxygen or water in the sample holder. For steady-state measurements a Müller-Elektronik-Optik SVX1450 Xe lamp or an IK3552R-G He-Cd continuous laser (325 nm) were used as excitation source, whereas a microsecond pulsed lamp was employed for recording the lifetime measurements. Photographs of irradiated single-crystals and polycrystalline samples were taken at room temperature in a micro-PL system included in an Olympus optical microscope illuminated with a Hg lamp. Time-resolved emission spectra were recorded using excitation and emission band-pass of 5 nm and 2.5 nm, respectively.

X-ray Diffraction. X-ray data collection of suitable single crystals of compounds were done at 100(2) K on a Bruker VENTURE area detector equipped with graphite monochromated Mo-Kα radiation (λ = 0.71073 Å) by applying the ω-scan method. The data reduction were performed with the APEX2[27] software and corrected for absorption using SADABS.[28] Crystal structures were solved by direct methods using the SIR97 program[29] and refined by full-matrix least-squares on F^2 including all reflections using anisotropic displacement parameters by means of the WINGX crystallographic package.[30,31] All hydrogen atoms were included as fixed contributions riding on attached atoms with isotropic thermal displacement parameters 1.2 times or 1.5 times those of their parent atoms for the organic ligands. Attempts to solve disorder problems with the DMF crystallization molecule failed in all compounds. Instead, a new set of

F^2 (hkl) values with the contribution from the solvent molecule withdrawn were obtained by the SOLVENT MASK procedure implemented in Olex2 v1.2 crystallographic package.[32] Details of the structure determination and refinement of compounds are summarized in Table 1. Crystallographic data for the structures reported in this paper have been deposited with the Cambridge Crystallographic Data Center as supplementary publication nos. CCDC 1942013-14 for compounds. Copies of the data can be obtained free of charge on application to the Director, CCDC, 12 Union Road, Cambridge, CB2 1EZ, U.K. (Fax: +44-1223-335033; e-mail: deposit@ccdc.cam.ac.uk or http://www.ccdc.cam.ac.uk).

Table 1. Crystallographic data and structure refinement details for all compounds.

Compound	**1**	**2**
Chemical formula	$C_{17}H_{15}N_6O_3Zn$	$C_{16}H_{15}N_4O_3Zn$
CCDC	1942013	1942014
M/g mol^{-1}	416.72	376.69
T/K	100 K	100 K
Cryst. syst.	Monoclinic	Orthorhombic
Space group	*C*2/*c*	*Pccn*
a (Å)	16.629(3)	16.8684(9)
b(Å)	17.930(4)	12.9147(7)
c(Å)	13.887(3)	14.8470(7)
β (°)	100.484(10)	90
V/ Å^3	4098.8(14)	3234.4(3)
Z	8	8
ρ/g cm^{-3}	1.469	1.547
μ/mm^{-1}	1.234	1.541
S(GOF)[a]	1.149	1.102
R[1>2*σ*(I)][b]	0.1222	0.0957
wR^2 [1>2*σ*(I)][c]	0.3276	0.2078

[a] $S = [\Sigma w(F_0^2 - F_c^2)^2 / (N_{obs} - N_{para}m)]^{1/2}$ [b] $R_1 = \Sigma||F_0|-|F_c|| / \Sigma|F_0|$ [c] $wR^2 = [\Sigma w(F_0^2 - F_c^2)^2 / \Sigma wF_0^2]^{1/2}$
$w = 1/[\sigma^2(F_0^2) + (aP)^2 + bP]$ where $P = (\max(F_0^2,0) + 2F_c^2)/3$

Computational details. PL spectra were calculated by means of TD-DFT using the Gaussian 09 package,[33] using the Becke three parameter hybrid functional with the non-local correlation

functional of Lee-Yang-Parr (B3LYP)[34-36] along with 6-311G++(d,p) basis set[37] was adopted for all atoms but for the central zinc cation, for which the LANL2DZ[38-40] basis set along with the corresponding effective core potential (ECP) was used. The 40 lowest excitation states were calculated by the TD-DFT method. Results were analyzed with GaussSum program package[41] and molecular orbitals plotted using GaussView 5.[42]

Results and Discussion

The solvothermal reaction between 1-H-indazole-5-carboxylic acid and the corresponding pyridine derivative ligand, with zinc acetate in H_2O:DMF, produces two new MOF materials (**1** and **2**) based on dimeric Secondary Building Units, in which the structures present interpenetration. Activation of MOFs **1** and **2** was performed by heating the washed material at 150ºC for 2 h. Crystallinity of desolvated materials was confirmed by Powder X-ray Diffraction (PXRD) (Figs. S1 and S2) whereas thermogravimetric analysis (TGA) was consistent with the elimination of solvent molecules (Figs. S3 and S4).

Structural description of $\{[Zn(5\text{-inca})(pbptz)_{0.5}]\cdot 1.5\ DMF)\}_n$ (1).

Compound **1** crystallizes in the *C*2/*c* monoclinic space group and the crystal structure consists on zinc(II) atoms linked through pbptz and 5-inca co-ligands, which afford large connectivity resulting in an open 3D framework.

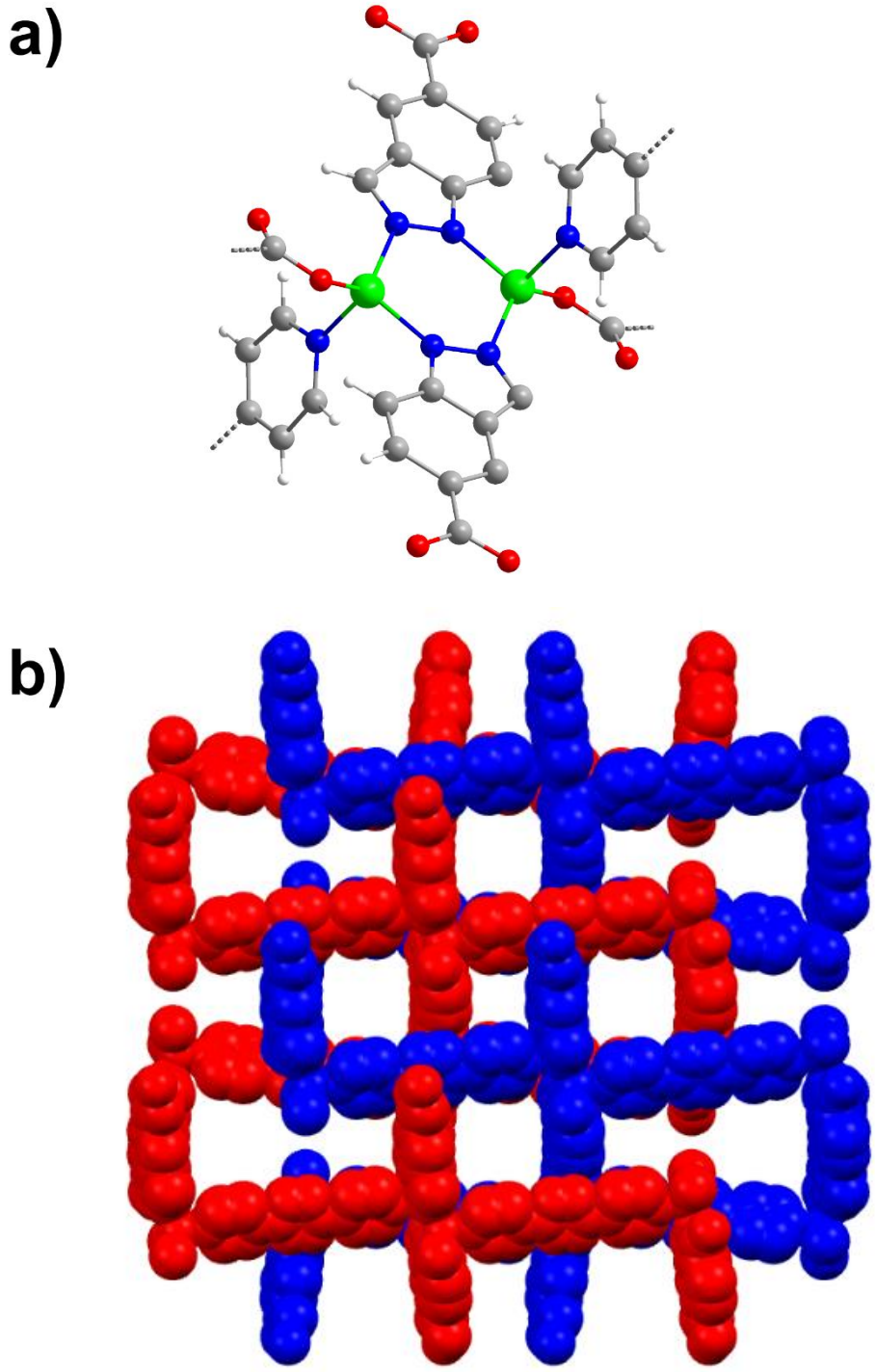

Figure 1. Crystal structure of compound **1**: **a)** fragment containing the SBU and **b)** perspective view showing the perpendicular disposition of the pillaring pbptz linkers with regard to Zn/5-inca layers. Colour code: zinc, green; oxygen, red; nitrogen, blue; carbon, grey; hydrogen, white.

The asymmetric unit of the crystal structure consists of a Zn1 atom, one 5-inca ligand and half of pbptz linker. The metal centre exhibits a N_3O tetrahedral coordination environment (Figure 1a) that is established by two nitrogen atoms from two symmetry related indazole rings, one nitrogen atom pertaining to pbptz ligand and one oxygen from the carboxylate group of a third 5-inca ligand. Continuous Shape Measures performed corroborate the low distorted tetrahedral shape (S_T = 0.67) of the coordination shell (see ESI). 5-inca exhibits the novel tridentate coordination mode showed in Scheme 1 (right), which allows it linking to two zinc(II) atoms through the nitrogen atoms pertaining to the indazole ring (N1A and N2A atoms) to eventually form dinuclear secondary building units (SBUs). Within these units, the metal atoms are slightly placed out of the planes delimited by indazole moieties (0.073 Å), in such a way that the resulting six-member ring imposes a Zn···Zn distance of 3.548 Å. Each building dinuclear unit connects to six neighbouring ones through both 5-inca ligands and pbptz linkers. On the one hand, the SBU joins to two adjacent units through the carboxylate moieties of four 5-inca ligands, two of which are coplanar and define the SBU of reference whereas the remaining two belong to other SBUs, yielding Zn/5-inca layers along the crystallographic *bc* plane. On the other hand, two pbptz pillaring linkers that arise almost perpendicularly from the central six-member ring of the SBU (with an angle of 76.5°) connect to the two remaining SBUs, thus establishing the 3D structure of the MOF (Figure 1b). Taking into account the connectivity achieved among SBUs, which may be considered as 6-connected nodes from the topological point of view, the framework resembles that exhibited by the well-known isoreticular family of MOF-5, in good agreement with the topological analysis performed with TOPOS software which confirms that herein described MOF possesses a ***pcu***

network with the ($4^{12}\cdot6^3$) point symbol (Figure 2).[43,44] The length of both connectors and the topology of the framework drive the growth of an almost empty architecture with so large accessible volume that admits the occurrence of a second network in the crystallization. Therefore, the porosity of the resulting two-fold interpenetrated structure is reduced though it still leaves a substantially large 2D void system in within that accounts for the 44.1% of the unit cell volume.[45] Despite the large solvent accessible volume contained in the structure, it must be highlighted that the pore network is not regular, but it contains large tubular channels with an approximate section of 7 Å, whereas the latter are cross-linked through narrow windows with apertures of 1.7–2.7 Å. This fact explains the limited gas adsorption capacity of the MOF, involving no N_2 adsorption capacity at low pressures. Instead, the microporous nature of the MOF was confirmed by CO_2 sorption isotherms (see Figure S15), revealing that compound **1** adsorbs 0.9 mmol/g of CO_2 at 273 K and 600 kPa and 0.34 mmol/g of CO_2 at 273 K and 2570 kPa, values which are lower than those of other recently reported MOFs. (M. Ding, R. W. Flaig, H.-L. Jiang, O. M. Yaghi, Chem. Soc. Rev. 2019, 48, 2783-2828; P. G. Boy et al. Nature, 2019, 576, 253-256) A careful analysis of the interpenetration occurring in the structure reveals that both frameworks are weakly bound to each other, finding no remarkable interactions apart from C–H$\cdots\pi$ interactions between indazole and pbptz ligands involving some kind of lateral interactions among their π clouds, which should be translated into a flexible character.

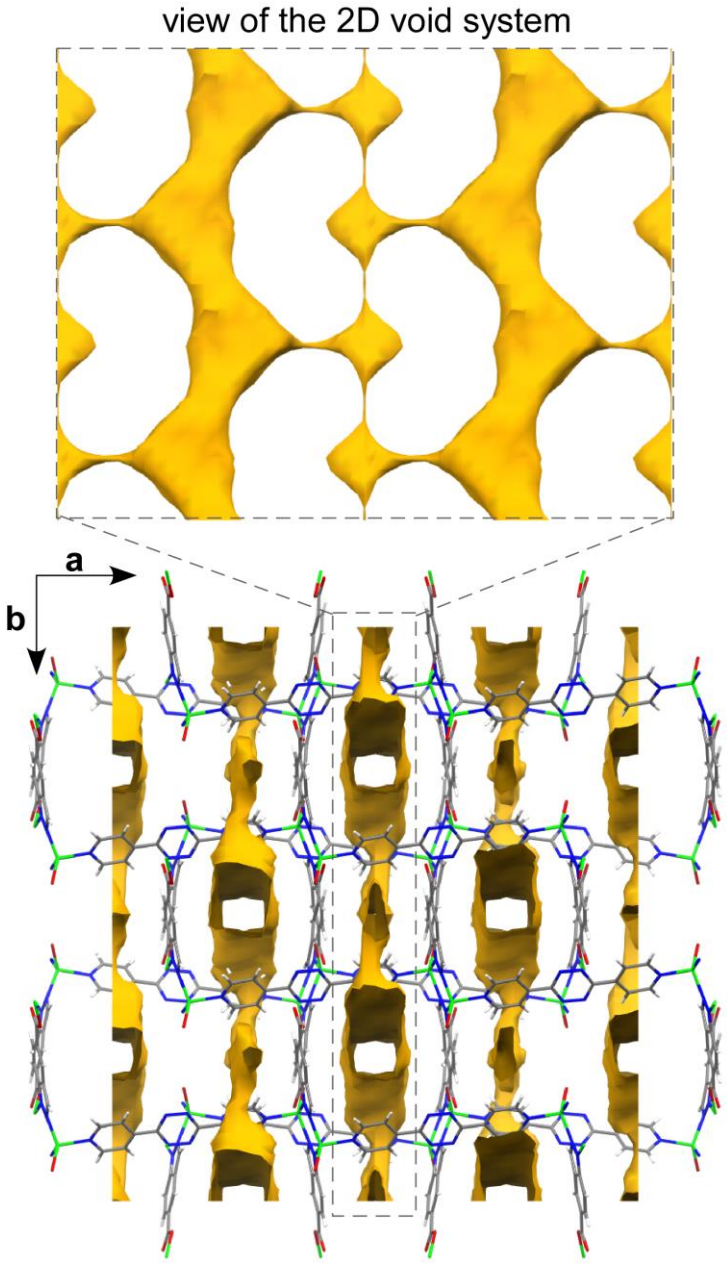

Figure 2. Perspective view of compound **1**. Hydrogen atoms have been omitted for clarity.

Structural description of {[Zn(5-inca)(4,4-bipy)$_{0.5}$]·DMF}$_n$ (2).

Compound **2** crystallizes in the orthorhombic *Pccn* space group and possesses an isoreticular 3D framework where pbptz linkers are replaced by 4,4-bipy. 5-inca exhibits a similar coordination pattern detailed for the previous material (right-hand side of Scheme

I), which forms dinuclear SBUs owing to the coordination of nitrogen atoms pertaining to the indazole ring to two zinc(II) atoms (Figure 3a). Three significant differences are found in this dinuclear unit compared to that of the previous compound: i) the carboxylate moiety of 5-inca ligand is slightly moved to bite the zinc atom (bringing a semi-coordination of O2A atom, Zn···O2A of 2.73 Å), despite of which the coordination environment is best described as a tetrahedron in view of the low distortion with regard to the ideal polyhedron (S_T = 0.413, see Table S1); ii) Zn atoms are more coplanar with regard to the plane established by the aromatic rings (which is dropped to 0.029 Å) and iii) the intradinuclear Zn···Zn distance is enlarged to 3.657 Å. It must be highlighted that both changes are clearly derived from the change of the pillaring linker which, being considerably shorter than pbptz (the Zn···Zn bond distance is reduced from 15.2 to 11.2 Å), modulates the flexibility of the framework.

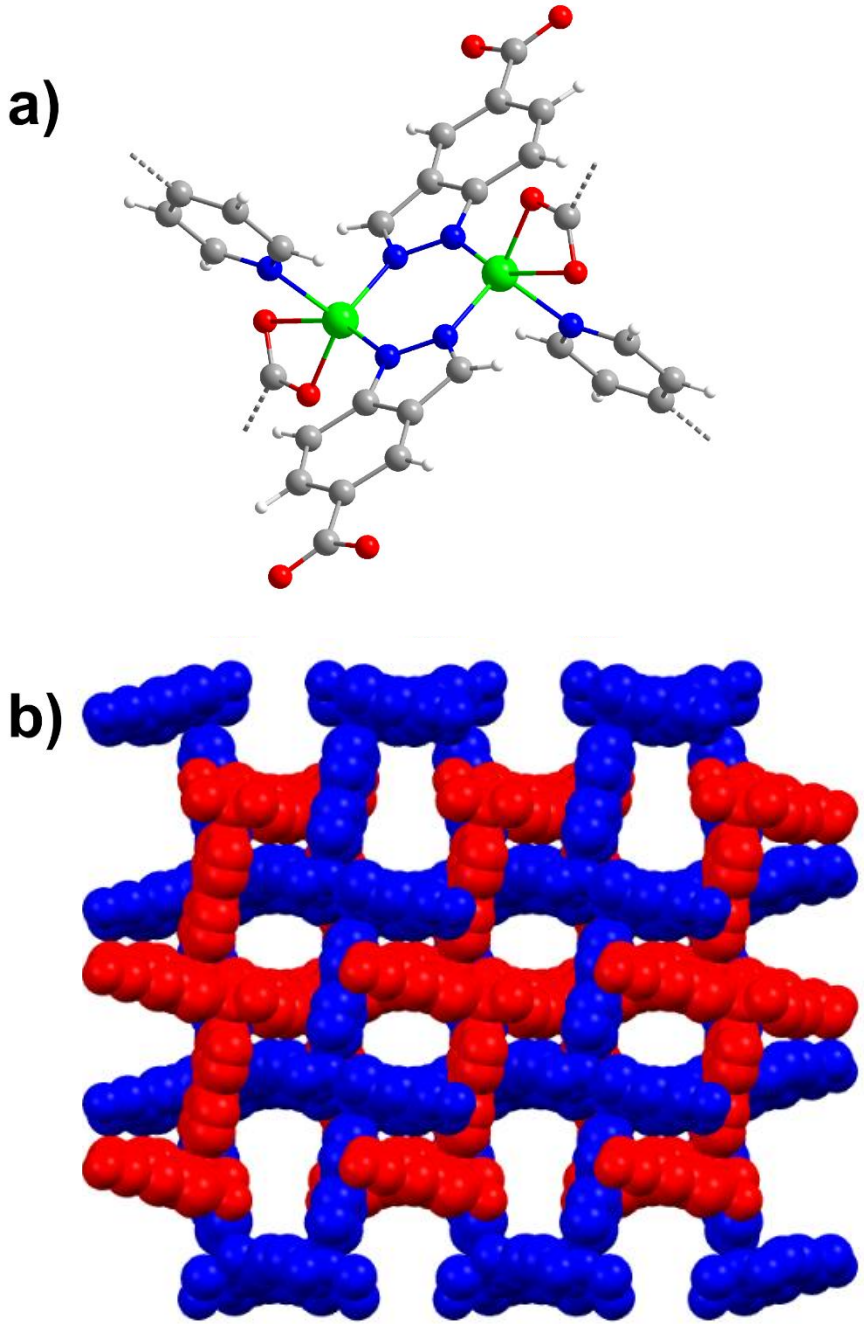

Figure 3. a) SBU of the structure of compound **2** and **b)** crystal packing of the compound showing the two-fold interpenetration.

As a consequence of the mutual displacement between the subnets, the free volume enclosed in the structure is shaped in the form of one-dimensional microchannels (with an irregular tubular shape containing wide and narrow sections of 4.3 and 1.6 Å) and accounts for 32.4% of the unit cell volume (Figure 4). The microporous nature of the MOF was confirmed by CO_2 sorption (see Figure S15), revealing that compound **2** adsorbs more CO_2 that compound **1**: 2.0 mmol/g CO_2 at 273 K and 600 kPa and 3.01 mmol/g CO_2 at 273 K and 2570 kPa.

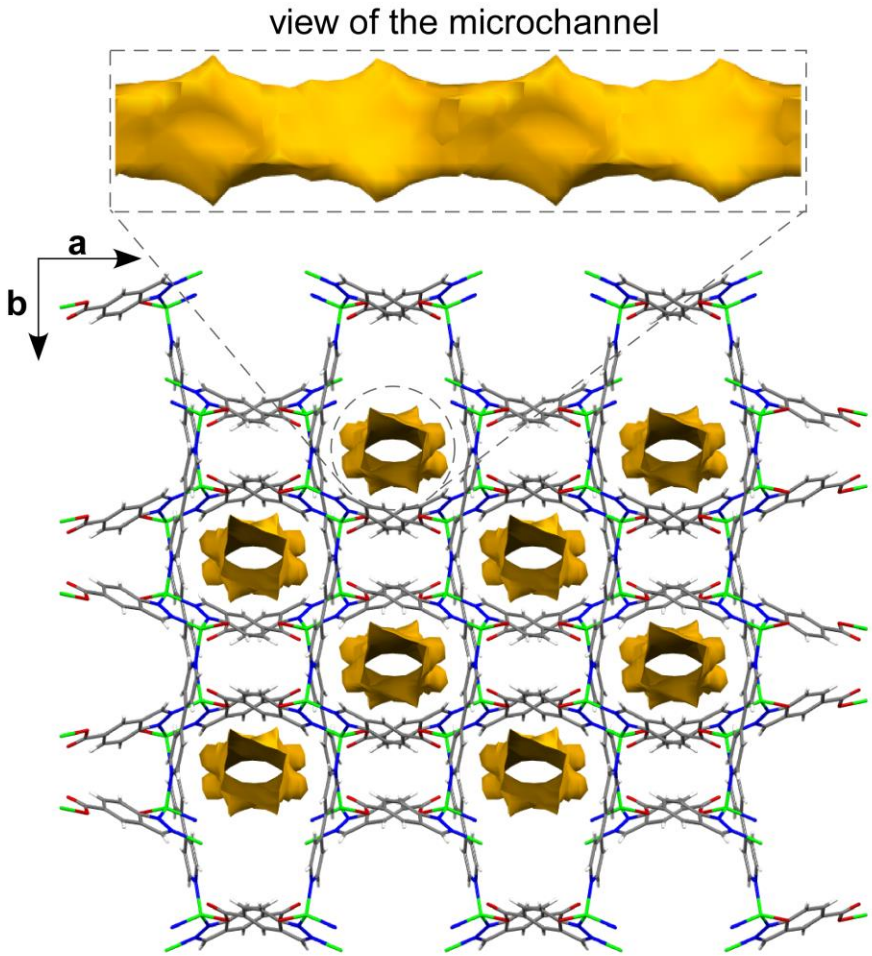

Figure 4. Perspective view of compound **2**. Hydrogen atoms have been omitted for clarity. Colour code: Zinc, light steel blue; oxygen, red; nitrogen, blue; carbon, grey; chloride, green.

Photoluminescence Properties.

The metal-organic nature of these materials, based on 3D frameworks containing ligands with π-conjugated systems (some of which are also decorated with carboxylate groups that are coordinated to closed-shell metal ions such as zinc(II)) make them suitable to exhibit photoluminescence (PL) in solid state. Under monochromatic UV light excitation (λ_{ex} = 325 nm), the room temperature emission spectrum of compound **1** consists of two main and one minor broad bands. A first main band is centred at 374 nm, followed by that located at 440 nm with a shoulder at 420 nm, which dominates the entire spectrum (Figure 5a). Finally, a less intense band is shown to peak at ca. 620 nm. It is worth mentioning that the two main bands are similar to the bands corresponding to each individual ligand, since free 5-inca and pbptz show emission bands at λ_{em} = 371 and 430/460 nm, respectively. Instead, the last less intense band, not directly related with the emissions centred on the ligands, may be ascribed to the formation of an exciplex among the π clouds of the aromatic rings of 5-inca and pbptz ligands pertaining to different subnets, although the participation of non-localized DMF molecules should not be discarded.[21,46] The subtle shifts observed for the bands with respect to free ligands can be attributed to the coordination effect, as previously observed for other zinc-based MOFs.[47,48]

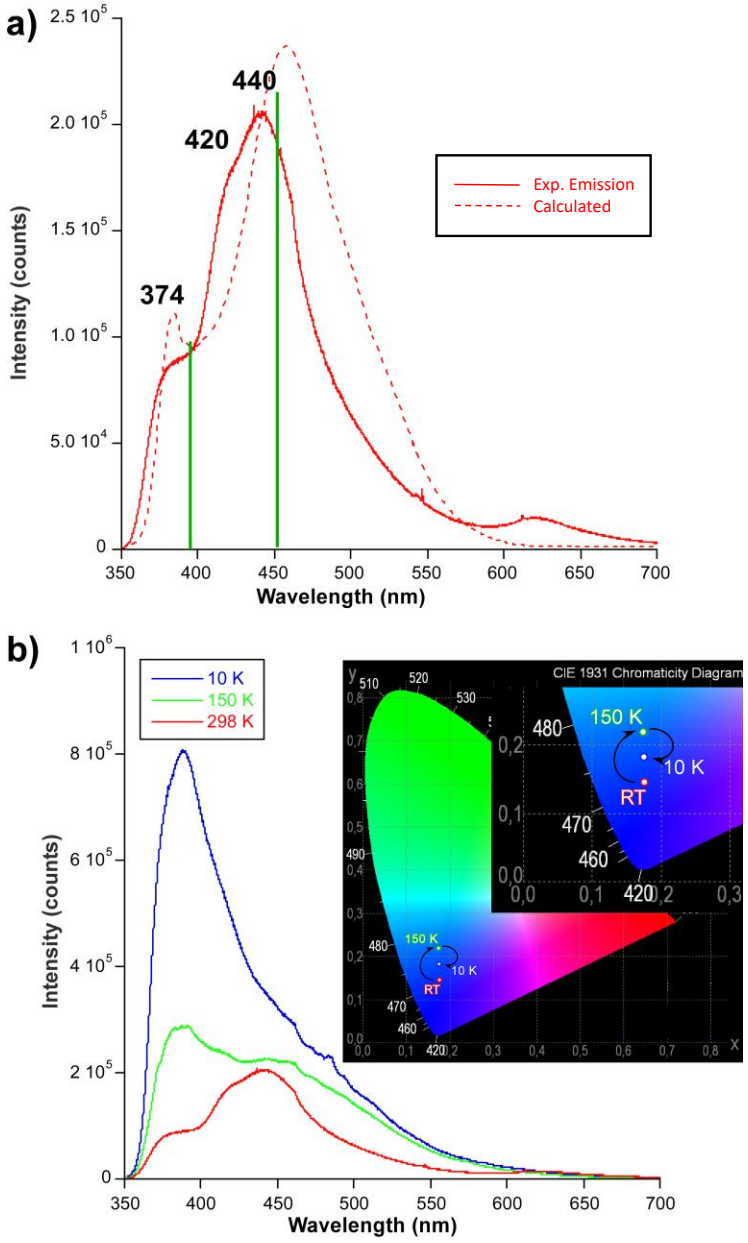

Figure 5. a) Room temperature experimental (solid red line) and TD-DFT calculated (dotted red line) steady-state emission spectra of compound **1**. Black numbers account for experimental emission maxima whereas main calculated main lines are represented as vertical green lines. **b)** Experimental emission spectra of **1** at variable temperature together with the thermochromic emission. Inset shows luminescent thermochromism represented in the CIE1931 chromaticity color coordinates.

In order to get deeper insights into the PL emission of **1**, TD-DFT calculations were conducted on a suitable model taken from its X-ray structure (model 1 hereafter, see Figure S5). As shown

in Figure 5a, after a vertical excitation at 320 nm proceeding through the HOMO – 5 → LUMO + 2 electronic transition (which represents the main excitation line and resembles the experimental λ_{ex} of 325 nm, see ESI), the calculated emission spectrum reproduces fairly well the experimental one, showing a wide band with two maxima peaking at 398 and 451 nm ascribed to HOMO – 1 ← LUMO + 1 and HOMO ← LUMO + 1. It is worth noticing that this model, based on a monomeric molecule, is not able to reproduce the minor less-energetic band peaking at ca. 625 nm. Nonetheless, a model consisting of a 5-inca and a pbptz ligand pertaining to different subnets (model 3, see Figures S7–8) suggests that the latter emission might be derived from their weak interaction, confirming the occurrence of excimer. Taking into account the dominant π and π* character of these electronic transitions in addition to the participation of molecular orbitals extending over both 5-inca and pbptz ligands, the PL scenario of **1** is accurately described as LLCT. Figure 6 summarizes the global PL scenario for a better understanding of their main electronic transitions. As it is well known, the luminescence in MOFs is known to be quenched by the coupling of non-radiative molecular vibrations, such as aromatic C–H bonds present in both ligands,[49,50] with excited-to-ground state energy difference. Therefore, the sample was cooled down to low temperature to study such effect. Keeping the experimental setting unchanged for comparative purposes, the emission spectrum was measured at the lowest possible temperature (10 K) as well as at an intermediate temperature (150 K). Interestingly, apart from an obvious increase of the emitted signal, which rises by a 43% at 150 K and by a 300% at 10 K considering the absolute emission maxima, the two main bands (λ_{em} = 374 and 440 nm) invert progressively their relative intensity as the temperature is dropped since at 10 K the 374 nm band at RT is covering most of the spectrum whereas that at 440 nm is nearly undistinguishable and becomes a shoulder (Figure 5b). On its part, the minor band (λ_{em} = 625

nm) is not observed anymore, meaning that the excimer is disrupted as the temperature drops probably due to a relative displacement between subnets. Especially at 10 K, the emission band extends up to 600 nm showing a long tail and is shifted to λ_{em} = 388 nm in such a way that it can be considered to occupy an intermediate wavelength between those of free ligands. The evolution of the emission spectra brings a remarkable luminescent thermochromism in the compound, since the emission varies among different tones of blue.

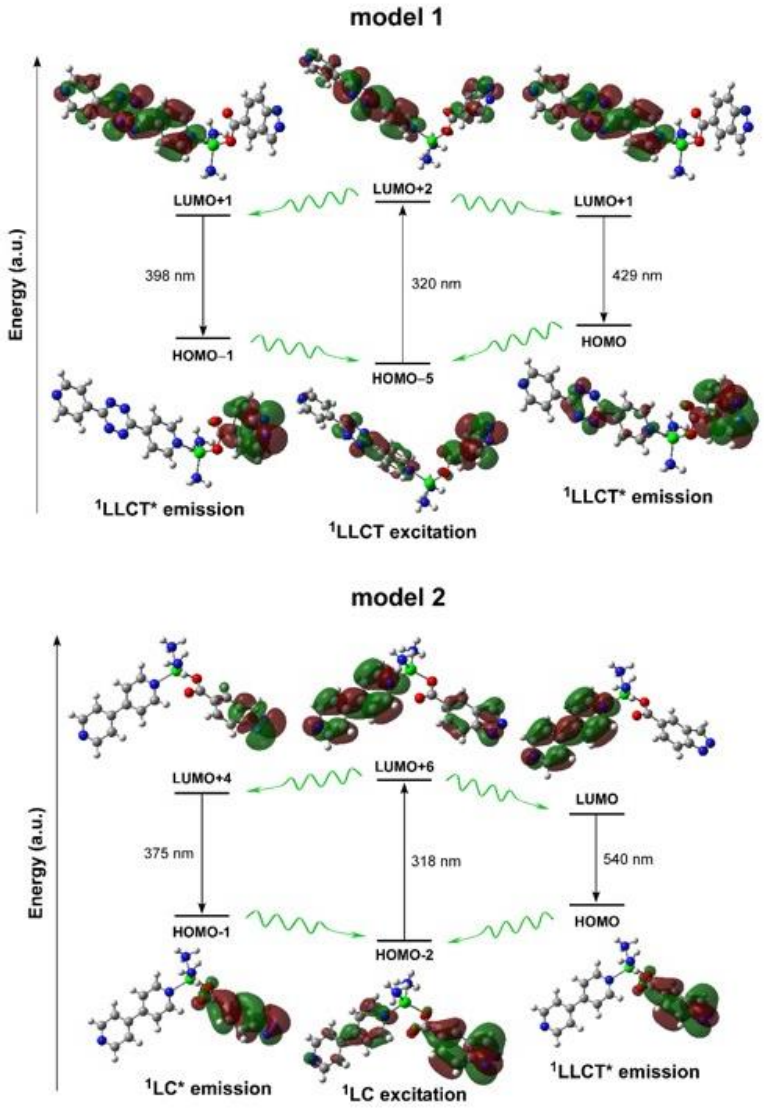

Figure 6. Diagram of the dominant MOs involved in the PL excitation and emission of models 1 and 2. Note that red and blue straight lines represent excitation and emission transitions, whereas undulated green lines account for vibrational relaxation processes.

On the other hand, under λ_{ex} = 325 nm excitation with a laser at RT, compound **2** shows two perfectly separated emission bands with their maximum centred at 380 and 535 nm, respectively (Figure 7). Conversely to **1**, compound **2** does not show any significant thermochromic effect (there is no change in the relative intensity of the maxima) but a strong increase in the absolute emission (integrated intensity) with the lowering of the temperature, which experiments an increment of 700% (see Figure S9). Despite the fact that one could a priori attribute the presence of two bands to the intra-ligand emission of 5-inca and bipy molecules, a similar band is only observed for the first ligand (λ_{em} = 380 for **2** and 371 nm for 5-inca), whereas the second band appears to be deeply red-shifted compared to the free bipy ligand emission (λ_{em} = 535 for **2** and 430 nm for bipy).[51]

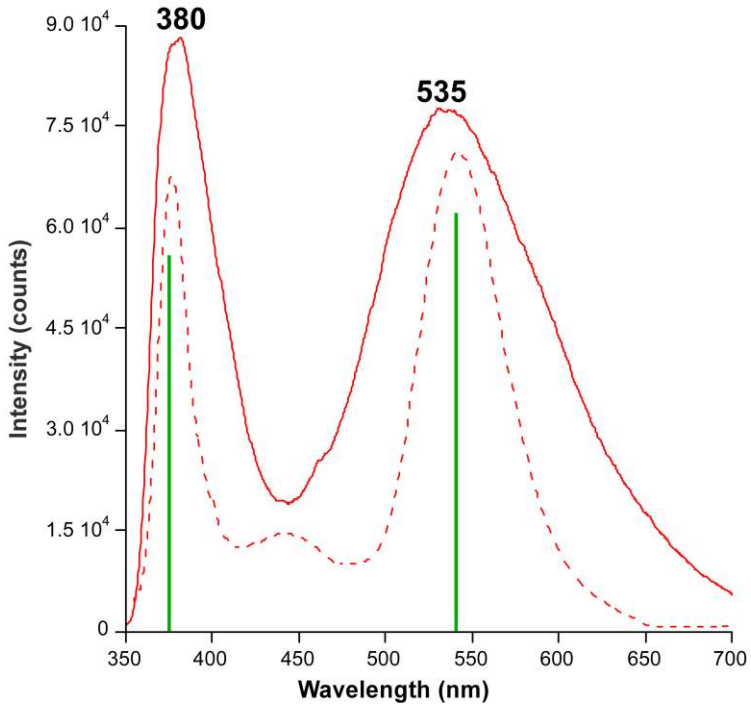

Figure 7. Comparison between room temperature experimental and calculated emission spectra of compound **2**. Black numbers and green lines represent the main experimental emission maxima and calculated vertical main lines.

A detailed analysis with TD-DFT methodology on a suitable model of **2** (model 2 hereafter) reveals a somewhat different PL scenario for this compound despite the similar nature of its ligands. On the one hand, the system is excited through two similar lines: a minor band at 302 nm corresponding to the HOMO – 5 → LUMO + 2 transition and the major band located at 318 nm described by the HOMO – 2 → LUMO + 6 transition. Given that the experimental spectrum is recorded with a λ_{ex} = 325 nm, it may be assumed that the excitation proceeds mainly through the latter transition. On the other hand, the radiative relaxation of **2** is governed by HOMO – 1 ← LUMO + 4 and HOMO ← LUMO transitions peaking at 375 and 540 nm, which fairly represent the two main emission bands. In agreement with the previous speculations, the first band is centred on the 5-inca ligand, which explains why it resembles the emission band displayed by the free ligand. Instead, the second band clearly corresponds to ligand-to-ligand charge transfer (LLCT) process involving the empty molecular orbitals (MOs) of the bipy and the filled MOs of 5-inca.

Though there is no previous report on LLP behaviour for CPs based on 5-inca ligand, in view of the long-lived phosphorescent emissions shown by zinc compounds based on similar aromatic ligands found in the literature, we decided to measure decay curves on both compounds.[17] To that end, the most representative emission wavelengths of the spectrum of **1** were monitored, i.e. the emission maxima (λ_{em} = 374 and 440 nm). The decay curves show a very rapid decrease of the signal, indicating that the emission proceeds through a fluorescent process. Though the decay at 374 nm is too rapid as to be analyzed (with a lifetime below the pulse of the lamp ≈ few μs), a weak but larger process could be discerned from the curve measured at 440 nm. The analysis by

means of an exponential expression gives a lifetime of about 4150 μs (see Figure S10), which may be regarded within the low limit of LLP (below the arbitrary value of 20 ms).[52] It was observed that lowering the temperature keeps the lifetime almost constant, where the subtle enlargement may be related with afore mentioned decrease of vibrational quenching ($\tau_{150\ K} \approx$ 6040 and $\tau_{10\ K} \approx$ 8590 μs). Instead, compound **2** presents a wavelength dependent emission scenario composed of a persistent fluorescent emission ($\tau_{fl} \approx 170$ μs) around the maximum of the first band ($\lambda_{em} = 380$ nm) and a phosphorescence emission ($\tau_{ph} \approx 200$ ms) around the high-wavelength band ($\lambda_{em} \approx 535$ nm, see Figure S11 and Table S2 in the ESI). Given their curvi-linear shape, all phosphorescence decay curves were fitted with two lifetime components so they were analysed with a multi-exponential expression [$I_t = A_0 + A_1\exp(-t/\tau_1) + A_2\exp(-t/\tau_2)$] that considers two lifetimes as usually performed for previous materials (see ESI). The pale blue and yellowish green colours displayed by **2** in the micro-PL photographs taken on crystals are a good indication of the fluorescent and phosphorescent emissions (see Figure 8). As observed in these photographs, the fluorescent signal observed under irradiation with UV light ($\lambda_{ex} \approx 365$ nm in the present case) shows a kind of luminescent waveguiding effect, since the emitted colour is only seen depending on the orientation of the crystals. This effect is not so common although it has already been described for other luminescent materials, for which crystals with an adequate refraction index and morphology as well as strong luminescence emission are required, in such a way that most of the light is confined within the crystal and emitted through a particular face.[53-57]

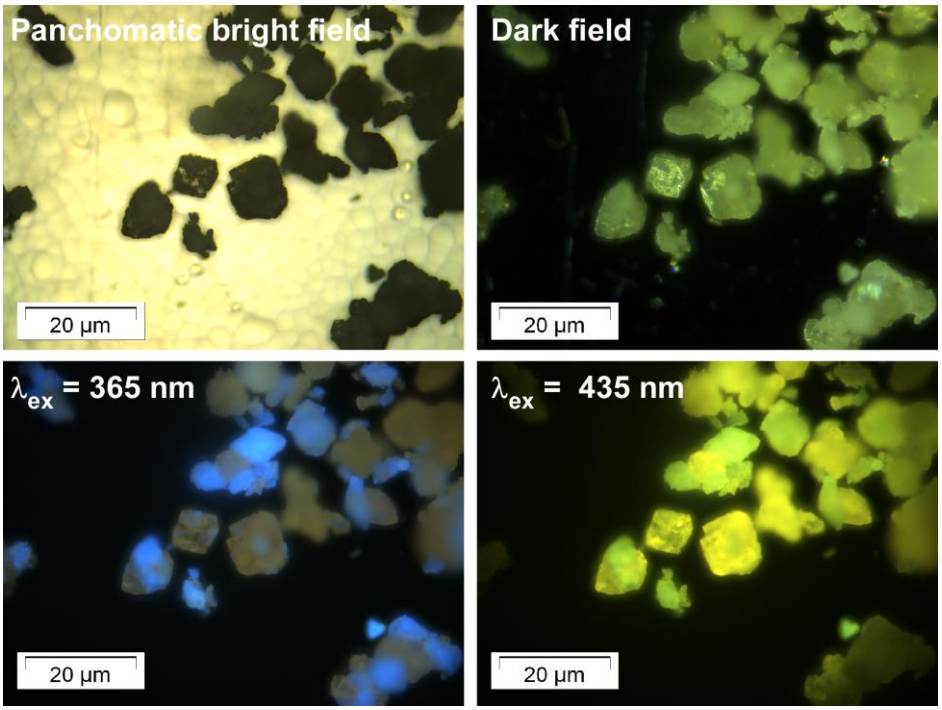

Figure 8. Room temperature micro-PL images for single-crystals of compound **2**.

The recorded lifetime of **2** is large enough as to be referred to as room temperature phosphorescence (RTP), which provides this compound with a very subtle greenish afterglow that is glimpsed when turning off laser beam. Dropping the temperature off to save non-radiative quenching does not bring any substantial on decay curves measured at the first emission maxima λ_{em} = 380 nm, but it promotes a substantial lengthening of the lifetime associated with the phosphorescent emission. In particular, at λ_{em} = 535 nm the lifetime enlarges progressively, mainly below 150 K, until it achieves a value of ca. 950 ms, which can be considered as an intermediate-to-large value for the CPs presenting LLP reported so far (Figure S12).[53-57] These results evidence the fluorescent/phosphorescent character of the MOF at low temperature, a fact that confirms that LCCT process occurring at the ligand is stabilized in the framework of the MOF such that both $S_0 \leftarrow S_1$ and $S_0 \leftarrow T_1$ transitions are enabled and enhanced. With the aim of better characterizing the phosphorescent emission, time-resolved emission spectra (TRES) were

recorded for **2** at low temperature, which confirmed that the persistent emission consists of a wide band centred at λ_{em} = 550 nm, close to the band measured at steady-state, thus explaining well the green-yelllowish afterglow shown when the UV excitation source is turned off (Figure 9). It is worth highlighting that the emitted light, yet it is weak as to be captured by a common camera, can be perfectly traced by the naked eye 4 seconds after having turned off the excitation source.

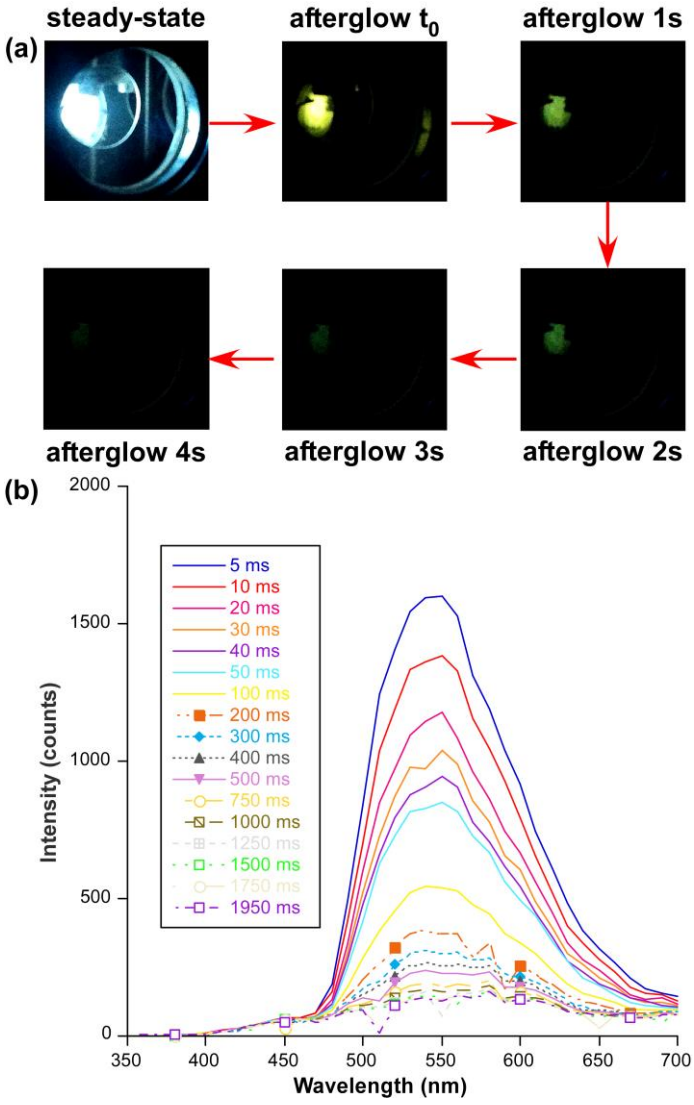

Figure 9. Photographs of the steady-state and afterglow emissions of compound 2 (top). TRES of compound **2** at 10 K at selected delays (λ_{ex} = 325 nm).

A calculation of the phosphorescent emission estimated from the DFT computed T_1 and S_0 electronic states (usually denoted as vertical excitation phosphorescent energy)[58] on model 2 gives a very good estimate of the experimentally measured band for compound **2** ($\lambda_{vert\text{-}phosp}$ = 507 vs λ_{ph} = 550 nm). This value can be taken as an approach to estimate the energy of the T_1 state in the compound assuming that the compound follows Kasha's rule.[59] A similar calculation performed on model 1 renders a $\lambda_{vert\text{-}phosp}$ = 470 nm, meaning that the T_1 state in compound **1**, conversely to **2**, is less energetic than the lowest-lying excited singlet state from which a radiative emission takes place ($S_0 \leftarrow S_1 \approx$ 440 nm). Therefore, this fact could a priori inhibit an intersystem crossing to populate the T_1 state that enables the occurrence of phosphorescence in **1** and, hence, explains why LLP is solely enhanced in compound **2**. Moreover, it cannot be discarded that weaker phosphorescence shown by **1** is also related to the less rigidity of pbptz ligand in the MOF, which clearly possesses more degrees of freedom compared to bipy ligand in **2**.

Conclusions

Two novel porous zinc based metal-organic frameworks consisting of indazole-5-carboxylate and 3,6-di(4-pyridinyl)-1,2,4,5-tetrazine for compound **1** or 4,4'-bipyridine like for **2** have been synthesized and characterized. Both MOFs present an isoreticular architecture with **pcu** topology that crystallizes as a doubly interpenetrated structure. This structural feature affords some flexibility to the frameworks and permits to modulate their porosity obtaining a 2D void system with narrow pore sections and 1D microchannels for **1** and **2**, respectively. Solid state photoluminescence measurements reveal that both

compounds provide intense blue emissions under irradiation with UV light which arise from charge transfers occurring between 5-inca and bipyridyl-like ligands as confirmed by TD-DFT calculations. Variable-temperature data indicate that compound **1** shows a remarkable thermochromism, which modulates the tonality of the emitted blue light provoked by the change in the relative intensity of the two main emission bands and an excimer formation/disruption between ligands belonging to different interpenetrated subnetworks. On its part, dropping down the temperature in **2** has no such effect yet it largely enhances its emission capacity, a fact that is particularly inferred from the occurrence of long-lasting phosphorescence that may be perceived by the naked eye (with an associated lifetime of ca 950 ms) below the temperature of liquid nitrogen. DFT calculations performed on these compounds point out to the relative energy of the excited singlet and triplet states as a probable source in the origin of sizeable phosphorescence solely in compound **2**, although the less rigidity of pbptz ligand of compound **1** compared to bipy in **2** may also have some influence.

ASSOCIATED CONTENT

Supporting Information. Additional figures of crystal structures and data, thermogravimetric analysis, powder X-ray diffraction analyses, photoluminescence spectra and lifetimes, TD-DFT computational results, and CIF files. This material is available free of charge via the Internet at http://pubs.acs.org.

AUTHOR INFORMATION

Corresponding Author

*E-mail: javier.cepeda@ehu.eus (J. C.)

*E-mail: guillermo.minguez@uv.es (G. M. E.)

*E-mail: antonio5@ugr.es (A. R. D.)

ACKNOWLEDGEMENTS

Financial support was given by Junta de Andalucía (Spain) (project number FQM-394 and FQM-1484), Red Guipuzcoana de Ciencia, Tecnología e Innovación (OF218/2018), University of the Basque Country (GIU 17/13), Gobierno Vasco/Eusko Jaurlaritza (IT1005-16), the Spanish Ministry of Science, Innovation and Universities (MCIU/AEI/FEDER, UE) (PGC2018-102052-A-C22, PGC2018-102052-B-C21, CTQ2017-89528-P cofinanced by FEDER and Excellence Unit María de Maeztu MDM-2015-0538 granted to ICMol), the Generalitat Valenciana (PROMETEU/2019/066) and the European Union (ERC-2016-CoG 724681-S-CAGE). G.M.E. and M.S. thank MICINN for a Ramón y Cajal and a Juan de la Cierva-Formación fellowships, respectively. The authors thank for technical and human support provided by SGIker of UPV/EHU and European funding (ERDF and ESF).

REFERENCES

(1) Chen, B.; Ma, S.; Zapata, F.; Fronczek, F. R.; Lobkovsky, E. B.; Zhou, H.-C. Rationally Designed Micropores within a Metal−Organic Framework for Selective Sorption of Gas Molecules. *Inorg. Chem*. **2007**, *46*, 1233-1236.

(2) Jeazet, H. B. T.; Staudt, C.; Janiak, C. A method for increasing permeability in O_2/N_2 separation with mixed-matrix membranes made of water-stable MIL-101 and polysulfone. *Chem. Commun*. **2012**, *48*, 2140-2142.

(3) Li, J.-R.; Sculley, J.; Zhou, H.-C. Metal-organic frameworks for separations. *Chem. Rev.* **2012**, *112*, 869-932

(4) Shang, J.; Li, G.; Singh, R.; Gu, Q.; Nairn, K. M.; Bastow, T. J.; Medhekar, N.; Doherty, C. M.; Hill, A. J.; Liu, J. Z.; Webley, P. A. Discriminative Separation of Gases by a "Molecular Tramdoor" Mechanism in Chabazite Zeolites. *J. Am. Chem. Soc.* **2012**, *134*, 19246-19253.

(5) Bourrelly, S.; Llewellyn, P. L.; Serre, C.; Millange, F.; Loiseau, T.; Fèrey, G. Different Adsorption Behaviors of Methane and Carbon Dioxide in the Isotypic Nanoporous Metal Terephthalates MIL-53 and MIL-47. *J. Am. Chem. Soc*. **2005**, *127*, 13519-13521.

(6) Yan, Y.; Yang, S. H.; Blake A. J.; Schroder, M. Studies on Metal-Organic Frameworks of Cu(II) with Isophthalate Linkers for Hydrogen Storage. *Acc. Chem. Res*. **2014**, *47,* 296-307.

(7) Pérez-Yáñez, S.; Beobide, G.; Castillo, O.; Fischer, M.; Hoffman, F.; Fröba, M.; Cepeda J.; Luque, A. Gas Adsorption Properties and selectivity in Cu^{II}/adeninato/carboxilato metal-Biomolecule Frameworks *Eur. J. Inorg. Chem.* **2012**, *2012,* 5921-5933.

(8) Farha, O. K.; Eyazici, I.; Jeong, N. C.; Hauser, B. G.; Wilmer, C. E.; Sarjeant, A. A.; Snurr, R. Q.; Nguyen, S. T.; Yazaydin, A.; Hupp, J. T. Metal-Organic Framework Materials with Ultra-High Surface Areas: Is the Sky the Limit? *J. Am. Chem. Soc.* **2012**, *134,* 15016-15021.

(9) Li, J.-R.; Kuppler, R. J.; Zhou, H.-C. Selective gas adsorption and separation in metal-organic frameworks. *Chem. Soc. Rev.* **2009**, 38, 1477-1504.

(10) Zhou, H.-C.; Kitagawa, S. Metal-Organic Frameworks (MOFs). *Chem. Soc. Rev.* **2014**, *43*, 5415-5418.

(11) Maurin, G.; Serre, C.; Cooper, A.; Férey, G. The new age of MOFs and of their porous-related solids. *Chem. Soc. Rev*. **2017**, *46*, 3104-3107.

(12) Cepeda, J.; Rodríguez-Diéguez, A. Tuning the luminescence performance of metal-organic frameworks based on d^{10} metal ions: from an inherent versatile behaviour to their response to external stimuli. *CrystEngComm*. **2016**, *18*, 8556-8573.

(13) Seco, J.M.; Fairen-Jimenez, D.; Calahorro, A.J.; Méndez-Liñán, L.; Pérez-Mendoza, M.; Casati, N.; Colacio E.; Rodríguez-Diéguez, A. Modular structure of a robust microporous MOF base don Cu_2 paddle-wheels with high CO_2 selectivity. *Chem.Commun*. **2013**, *49,* 11329-11331.

(14) Cepeda, J.; Pérez-Mendoza, M.; Calahorro, A.J.; Casati, N.; Seco, J.M.; Aragones-Anglada, M.; Moghadam, P.Z.; Fairen-Jimenez, D.; Rodríguez-Diéguez, A. Modulation of Pore shape and adsorption selectivity by ligand funtionalization in a series of “rob”-like flexible metal-organic frameworks. *J. Mater. Chem. A.* **2018**, *6*, 17409-17416.

(15) Li, H.-Y.; Wei, Y.-L.; Dong, X.-Y.; Zang, S.-Q.; Mak, T. C. W. Novel Tb-MOF Embedded with Viologen Species for Multi-Photofunctionality: Photochromism, Photomodulated Fluorescence, and Luminescent pH Sensing. *Chem. Mater.* **2015**, *27*, 1327-1331.

(16) Barbieri, A.; Accorsi, G.; Armaroli, A. Luminescent complexes beyond the platinum group: the d^{10} avenue. *Chem. Commun.* **2008**, 2185-2193.

(17) San Sebastian, E.; Rodríguez-Diéguez, A.; Seco, J. M.; Cepeda, J. Coordination Polymers with Intriguing Photoluminescence Behavior: The Promising Avenue for Greatest Long-Lasting Phosphors. *Eur. J. Inorg. Chem.* **2018**, 2155-2174.

(18) Rocha, J.; Brites, C. D. S.; Carlos, L. D. Lanthanide Organic Framework Luminescent Thermometers. *Chem.–Eur. J.* **2016**, *22*, 14782-14795.

(19) Han, Y.-H.; Tian, C.-B.; Li, Q.-H.; Du, S.-W. Highly chemical and thermally stable luminescent Eu_xTb_{1-x} MOF materials for broad-range pH and temperature sensors. *J. Mat. Chem. C* **2014**, *2*, 8065-8070.

(20) Brites, C. D. S.; Lima, P.; Silva, N. J. O.; Millán, A.; Amaral, V. S.; Palacio, F.; Carlos, L. D. Lanthanide-based luminescent molecular thermometers. *New J. Chem.* **2011**, *35*, 1177-1183.

(21) Allendorf, M. D.; Bauer, C. A.; Bhaktaa, R. K.; Houk, R. J. T. Luminescent metal–organic frameworks. *Chem. Soc. Rev.* **2009**, *38*, 1330-1352.

(22) Lower, S. K.; El-Sayed, M. A. The Triplet State and Molecular Electronic Processes in Organic Molecules. *Chem. Rev.* **1966**, *66*, 199-241.

(23) Hawes, C.S.; Babarao, R.; Hill, M. RR.; White, K. F.; Abrahams, B. F.; Kruger, P.E. Hysteretic carbon dioxide sorption in a novel copper(II)-indazole-carboxylate porous coordination polymer. *Chem. Commun.* **2012**, *48*, 11558-11560.

(24) Botana, L.; Ruiz,J.; Seco, J.M.; Mota, A. J.; Rodríguez-Diéguez, A.; Sillanpää, R.; Colacio, E. Influence of the anions on the structure and magnetic properties of a series of bis(μ-diphenoxo)-bridged linear trinuclear copper(II) complexies: an experimental and theoretical study. *Dalton Trans*. **2011**, *40,* 12462-12471.

(25) Seco, J. M.; Pérez-Yáñez, S.; Briones, D.; García, J. A.; Cepeda, J.; Rodríguez-Diéguez, A. Combining Polycarboxylate and Bipyridyl-like Ligand in the Design of luminescent Zinc and Cadmium Based Metal-Organic Frameworks. *Cryst. Growth Des*. **2017**, *17,* 3893-3906.

(26) Qi, Y.-J.; Wang, Y.-J.; Li, X.-X.; Zhao, D.; Sun, Y.-Q.; Zheng, S.-T. Two d^{10} Metal−Organic Frameworks as Low-Temperature Luminescent Molecular Thermometers. *Cryst. Growth Des*. **2018**, *18*, 7383-7390.

(27) *Bruker Apex2*, Bruker AXS Inc., Madison, Wisconsin, USA, **2004**.

(28) Sheldrick, G.M. *SADABS*, Program for Empirical Adsorption Correction, Institute for Inorganic Chemistry, University of Gottingen, Germany, **1996**.

(29) Altomare, A.; Burla, M. C.; Camilla, M.; Cascarano, G. L.; Giacovazzo, C.; Guagliardi, A. Moliterni A. G. G.; Polidori, G.; Spagna, R. SIR97: a new toll for crystal structure determination and refinement. *J. Appl. Cryst.* **1999**, *32*, 115-119.

(30) Sheldrick, G. M. *SHELX-2014*, Program for Crystal Structure Refinement, University of Göttingen, Göttingen, Germany, **2014**.

(31) Farrugia, L. J. WinGX suite for small-molecule single-crystal crystallography. *J. Appl. Cryst.* **1999**, *32,* 837-838.

(32) Dolomanov, O. V.; Bourhis, L. J.; Gildea, R. J.; Howard J. A. K.; Pushmann, H. *J. Appl. Cryst.* **2009**, *42*, 339-341.

(33) Frisch, M. J.; Trucks, G. W.; Schlegel, H. B.; Scuseria, G. E.; Robb, M. A.; Cheeseman, J. R.; Scalmani, G.; Barone, V.; Mennucci, B.; Petersson, G. A.; Nakatsuji, H.; Caricato, M.; Li, X.; Hratchian, H. P.; Izmaylov, A. F.; Bloino, J.; Zheng, G.; Sonnenberg, J. L.; Hada, M.; Ehara, M.; Toyota, K.; Fukuda, R.; Hasegawa, J; Ishida, M.; Nakajima, T.; Honda, Y.; Kitao, O.; Nakai, H.; Vreven, T.; Montgomery Jr. J. A.; Peralta, J. E.; Ogliaro, F.; Bearpark, M.; Heyd, J. J.; Brothers, E.; Kudin, K. N.; Staroverov, V. N.; Kobayashi, R.; Normand, J.; Raghavachari, K.; Rendell, A.; Burant, J. C.; Iyengar, S. S.; Tomasi, J.; Cossi, M.; Rega, N.; Millam, J. M.; Klene, M.; Knox, J. E.; Cross, J. B.; Bakken, V.; Adamo, C.; Jaramillo, J.; Gomperts, R.;. Stratmann, R. E, Yazyev, O.; Austin, A. J.; Cammi, R.; Pomelli, C.; Ochterski, J. W.; Martin, R. L.; Morokuma, K.; Zakrzewski, V. G.; Voth, G. A.; Salvador, P.; Dannenberg, J. J.; Dapprich, S.; Daniels, A. D.; Farkas, O.; Foresman, J. B.; Ortiz, J. V.; Cioslowski J.; Fox, D. J. *Gaussian 09, revision A.02*, Gaussian, Inc., Wallingford, CT, **2009**.

(34) Becke, A. D. Density-functional thermochemistry. III. The role of exact exchange. *J. Chem. Phys.* **1993**, 98, 5648-5652.

(35) Miehlich, B.; Savin, A.; Stoll, H; Preuss, H. Results obtained with the correlation energy density functional of becke and Lee, Yang and Parr. *Chem. Phys. Lett.* **1989**, *157,* 200-206.

(36) Lee, C.; Yang, W.; Parr, R. G. Development of the Colle-Salvetti correlation-energy formula into a functional of the electron density. *Phys. Rev. B*. **1988,** *37*, 785-789.

(37) Noodleman, L.; Case, D. A.; Aizman, A. Broken symmetry analysis of spin coupling in iron-sulfur clusters. *J. Am. Chem. Soc.* **1988,** *110,* 1001-1005.

(38) Hay, P. J.; Wadt, W. R. Ab initio effective core potentials for molecular calculations. Porentials for the transition metal atoms Sc to Hg. *J. Chem. Phys.* **1985**, *82,* 270-283.

(39) Wadt, W. R.; Hay P. J. Ab initio effective core potentials for molecular calculations. Porentials for main group elements Na to Bi. *J. Chem. Phys.* **1985**, *82,* 284-298.

(40) Hay, P. J.; Wadt, W. R. Ab initio effective core potentials for molecular calculations. Porentials for K to Au including the Outermost core orbitals. *J. Chem. Phys.* **1985**, *82*, 299-310.

(41) O'Boyle, N. M.; Tenderholt, A. L.; Langner, K. M. cclib: A library for package-independent computational chemistry algorithms. *J. Comput. Chem.* **2008**, *29,* 839-845.

(42) Dennington, R.; Keith, T.; Millam, J. *GaussView, Version 5,* Semichem Inc., Shawnee Mission: KS, **2009**.

(43) *TOPOS Main Page*, http://www.topos.ssu.samara.ru (accessed February 14, 2019).

(44) Blatov, V.A.; Shevchenko, A. P.; Proserpio, D. M. Applied Topological Analysis of Crystal Structures with the program Package ToposPro. *Cryst. Growth Des.* **2014**, *14,* 3576-3586.

(45) Spek, A. L. Structure validation in chemical crystallography. *Acta Cryst.* **2009**, *D65,* 148-155.

(46) Wagner, B. D.; McManus, G. J.; Moulton, B.; Zaworotko, M. J. *Chem. Commun.* **2002**, 2176–2177.

(47) Zheng, Q.; Yang, F.; Deng, M.; Ling, Y.; Liu, X.; Chen, Z.; Wang, Y.; Zhou, Y. A Porous Metal-Organic Framework Constructed from Carboxylate-Pyrazolate Shared Heptanuclear Zinc Clusters: Synthesis, Gas Adsorption, and Guest-Dependent Luminescent Properties. *Inorg. Chem.* **2013**, *52,* 10368-10374.

(48) Ren, H.-Y.; Han, C.-Y.; Qu, M.; Zhang, X.-M. Luminescent group 12 metal tetracarboxylate networks as probe for metal ions. *RSC Adv.* **2014**, *4,* 49090-49097.

(49) Eliseeva, S. V.; Pleshkov, D. N.; Lyssenko, K. A.; Lepnev, L. S.; Bünzli, J. C.; Kuzmina, N. P. Highly Luminescent and Triboluminescent Coordination Polymers Assemble from Lanthanide β-Diketonates and Aromatic Bidentate O-donor Ligands. *Inorg. Chem.* **2010**, *49*, 9300-9311.

(50) De Bettencourt-Dias, A.; Barber, P. S.; Viswanathan, S.; de Lill, D. T.; Rollett, A.; Ling, G.; Altun, S. Para-derivatized Pybox Ligands As Sensitizers in Highly Luminescent Ln(III) Complexes. *Inorg. Chem.* **2010**, *49,* 8848-8861.

(51) Mendiratta, S.; Lee, C.-H.; Lee, S.-Y.; Kao, Y.-C.; Chang, B.-C.; Lo, Y.-H.; Lu, K.-L. Structural Characteristics and Non-Linear Optical Behaviour of a 2-Hydroxynicotinate-containing Zinc-Based Metal-Organic Framework. *Molecules* **2015**, *20,* 8941-8951.

(52) Xue, P.; Wang, P.; Chen, P.; Yao, B.; Gong, P.; Sun, J.; Zhang, Z.; Lu, R. Bright persistent luminescence from pure organic molecules through a moderate intermolecular heavy atom effect. *Chem. Sci.* **2017**, 8, 6060-6065.

(53) Cepeda, J.; Pérez-Yáñez, S.; Beobide, G.; Castillo, O.; García, J. A.; Lanchas, M.; Luque, A. Enhancing luminescence properties of lanthanide(III)/pyrimidine-4,6-dicarboxylato system by solvent-free approach. *Dalton Trans.* **2015**, *44*, 6972-6986.

(54) Yang, X.; Lin, X.; Zhao, Y.; Zhao Y. S.; Yan, D. Lanthanide Metal-Organic Framework Microrods: Colored Optical Waveguides and Chiral Polarized Emission *Angew. Chem., Int. Ed.* **2017**, *56,* 7853-7857.

(55) Geburt, S., Lorke, M.; da Rosa, A. L.; Frauenheim, T.; Röder, R.; Voss, T.; Kaiser, U.; Heimbrodt, W.; Ronning, C. Intense Intrashell Luminescence of Eu-Doped Single ZnO nanowires at Room Temperature by Implantation Created Eu-O_i complexes. *Nano Lett.* **2014**, *14,* 4523-4528.

(56) Pajuelo-Corral, O.; Rodríguez-Diéguez, A.; García, J. A.; San Sebastian, E.; Seco, J. M.; Cepeda, J. Chiral coordination polymers based on d^{10} metal and 2-aminonicotinate with blue fluorescent/green phosphorescent anisotropic emissions. *Dalton Trans.* **2018**, *47*, 8746-8754.

(57) Gu F.; Yu, H.; Wang, P.; Yang, Z.; Tong, L. Light-Emitting Polymer Single Nanofibers via Waveguiding Excitation. *ACS Nano* **2010***, 4,* 5332-5338.

(58) Adamo C.; Jacquemin, D. The calculations of Excited-state properties with Time-Dependent Density Funtional Theory. *Chem. Soc. Rev.* **2013**, *42,* 845-856.

(59) Kasha, M. Characterization of electronic transitions in complex molecules. *Discuss. Faraday Soc.* **1950**, *9*, 14-19.